

AMGFormer: ADAPTIVE MULTI-GRANULAR TRANSFORMER FOR BRAIN TUMOR SEGMENTATION WITH MISSING MODALITIES

Chengxiang Guo¹, *Jian Wang¹, Junhua Fei¹, Xiao Li¹, Chunling Chen¹, Yun Jin²

¹Faculty of Information Engineering and Automation, Kunming University of Science and Technology

²Hepatobiliary & Pancreatic Surgery, First People's Hospital of Yunnan/KUST Affiliated Hospital

ABSTRACT

Multimodal MRI is essential for brain tumor segmentation, yet missing modalities in clinical practice cause existing methods to exhibit $>40\%$ performance variance across modality combinations, rendering them clinically unreliable. We propose AMGFormer, achieving significantly improved stability through three synergistic modules: (1) QuadIntegrator Bridge (QIB) enabling spatially adaptive fusion maintaining consistent predictions regardless of available modalities, (2) Multi-Granular Attention Orchestrator (MGAO) focusing on pathological regions to reduce background sensitivity, and (3) Modality Quality-Aware Enhancement (MQAE) preventing error propagation from corrupted sequences. On BraTS 2018, our method achieves 89.33% WT, 82.70% TC, 67.23% ET Dice scores with $<0.5\%$ variance across 15 modality combinations, solving the stability crisis. Single-modality ET segmentation shows 40-81% relative improvements over state-of-the-art methods. The method generalizes to BraTS 2020/2021, achieving up to 92.44% WT, 89.91% TC, 84.57% ET. The model demonstrates potential for clinical deployment with 1.2s inference. Code: <https://github.com/guochengxiangives/AMGFormer>.

Index Terms— Brain tumor segmentation, Missing modalities, Adaptive fusion, Multi-granular attention

1. INTRODUCTION

Brain tumors, particularly glioblastoma multiforme (GBM), represent one of the most lethal malignancies with median survival of 14-15 months and five-year survival rates below 5% [1]. Accurate segmentation is crucial for treatment planning and patient monitoring, yet clinical reality poses significant challenges. While Magnetic Resonance Imaging (MRI) employs four standard sequences—FLAIR, T1-weighted, T1-weighted contrast-enhanced (T1CE), and T2-weighted—to

capture complementary tumor characteristics[2], complete acquisition is frequently impossible: contrast agents are contraindicated in 5-10% of patients due to renal dysfunction or allergies [3], emergency settings demand rapid protocols, and retrospective studies encounter incomplete archives[4]. This creates a critical gap: automated segmentation systems struggle with missing modalities, showing significant performance degradation that limits clinical deployment[5].

Deep learning has transformed brain tumor segmentation, with CNN architectures like U-Net[6] and nnU-Net [7] achieving remarkable results—but only with complete modality sets. Recent advances specifically tackle the missing modality challenge through various strategies. Knowledge distillation methods[8] transfer information from complete to incomplete modality networks. Reconstruction-driven approaches like DRNet [9] employ deformation-aware strategies. Generative models including HeMIS[10] and U-HVED[11] synthesize missing modalities or learn shared representations. More recently, RFNet[12] employs region-aware fusion, SMU-Net [13] uses style matching, mmFormer [5] leverages transformers, methods like [14] model intra-modal asymmetry and inter-modal dependencies, and category-aware group self-support learning [15] enables mutual assistance. However, these methods fundamentally fail to solve the stability crisis: performance varies drastically across different modality combinations. The experiment of M2FTrans exhibits 45% variance (37.24-82.19% ET) across scenarios[16]. Previous studies report that HeMIS and U-HVED achieve only 10-20% DSC when T1CE is missing[17]. This instability—not just average performance—renders these methods clinically unusable, as physicians cannot trust systems whose predictions change dramatically based on available sequences.

The instability stems from three fundamental architectural flaws inherent in current approaches. First, static fusion mechanisms apply identical processing regardless of modality availability, causing unpredictable behavior when input distributions shift—a network trained expecting four modalities behaves erratically with only two. Second, absence of quality awareness means corrupted modalities propagate errors throughout the network, amplifying instability as a single motion-corrupted sequence can destabilize the entire predic-

*Corresponding author: Jian Wang, email: jianwang@kust.edu.cn. This work was supported by the Key Research and Development Program of Yunnan Province (No. 202402AA310056), the Special Fund for the Central Government to Guide Local Science (No. 202407AB110003), the National Natural Science Foundation of China under Grant (No. 62366057), Theopen project of the Key Laboratory of Media Convergence in Yunnan Province (No. 220245204).

tion. Third, uniform attention dilutes focus across the entire volume, making models hypersensitive to missing modality patterns in the 85%-95% background regions rather than robust to changes in the 5%-15% tumor area where stability matters most.

To achieve clinical-grade stability, we propose Adaptive Multi-Granular Transformer that fundamentally reimagines fusion architecture for robust performance across all modality scenarios. Our key innovations include: (1) QuadIntegrator Bridge (QIB) for spatially-adaptive fusion that dynamically adjusts to available modalities, maintaining consistent predictions regardless of input combinations; (2) Multi-Granular Attention Orchestrator (MGAO) for efficient sparse attention focusing on pathological regions, reducing sensitivity to background variations; (3) Modality Quality-Aware Enhancement (MQAE) for quality-aware cross-modal enhancement that adaptively handles modality-specific artifacts and missing sequences. Our method achieves significantly improved stability—the missing piece for clinical deployment: (1) <0.5% variance ET across 15 modality combinations versus >40% in existing methods, ensuring consistent predictions regardless of available sequences; (2) robust single-modality performance proving each modality is fully utilized rather than creating dependencies; (3) state-of-the-art accuracy reaching 84.57% ET on BraTS2021, consistently high across three benchmarks, with 1.2s inference time, enabling reliable clinical deployment where modality availability is unpredictable.

2. METHOD

2.1. Overview

Fig. 1 shows our multi-branch encoder-decoder architecture processing four MRI modalities through parallel encoders. At the bottleneck, MGAO first processes each modality independently for intra-modal refinement, then applies cross-modal attention on concatenated features to capture inter-modal dependencies. During decoding, MQAE performs quality-aware compensation while QIB enables spatially-adaptive fusion, producing segmentation maps via multi-scale supervision. During training, we employ dual supervision with both the fused decoder and auxiliary modality-specific decoders to enhance feature learning[5, 9].

2.2. QuadIntegrator Bridge (QIB)

Traditional fusion applies uniform weights across the entire volume, ignoring that different modalities excel at different tissues (e.g., T1CE for tumor enhancement, FLAIR for edema). As shown in Fig. 2, QIB learns spatially-adaptive fusion weights that dynamically adjust based on local tissue characteristics. Given four modality features $\{X_m^i\}_{m=1}^4$ at scale i , QIB performs adaptive fusion through:

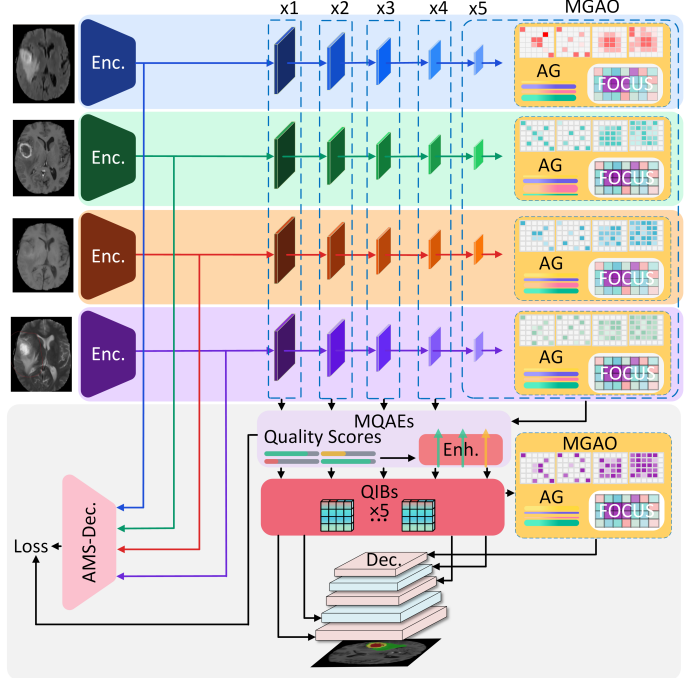


Fig. 1. AMGFormer architecture. Four MRI modalities processed through encoders (Enc.) with dual-stage MGAO (intra- then inter-modal attention, AG: Adaptive Aggregation). MQAE provides enhancement (Enh.) and quality scores. QIB enables adaptive fusion in decoder (Dec.). AMS-Dec.: auxiliary modality-specific decoders.

Feature Alignment. First, Project modalities into common space: $\hat{X}_m^i = \text{ReLU}(\text{BN}(\text{Conv}_{1 \times 1 \times 1}(X_m^i)))$, aligning different feature distributions from independent encoders.

Synergistic Integration Module (SIM). The aligned features then flow into SIM, which capture inter-modal complementarity through $3 \times 3 \times 3$ convolutions with batch normalization, reducing channels from $4C_i$ to C_i while learning complementary patterns.

Spatially-Adaptive Fusion Controller (SAFC). Using SIM’s integrated features, SAFC generate spatially-varying importance scores producing $W^i \in \mathbb{R}^{B \times 4 \times H \times W \times D}$. Crucially, we use ReLU with batch normalization instead of Softmax—while Softmax forces $\sum_m W_m = 1$ redistributing missing modality weights, ReLU allows selective suppression, naturally handling missing sequences.

Weighted Fusion. Finally, we compute spatially-adaptive fusion: $F_{\text{fused}}^i = \sum_{m=1}^4 W_m^i \odot \hat{X}_m^i$, enabling the network to automatically learn that T1CE dominates for tumor core while FLAIR excels at edema boundaries.

2.3. Multi-Granular Attention Orchestrator (MGAO)

Standard 3D self-attention treats all voxels equally despite brain tumors comprising 5-15% of volume, wasting compu-

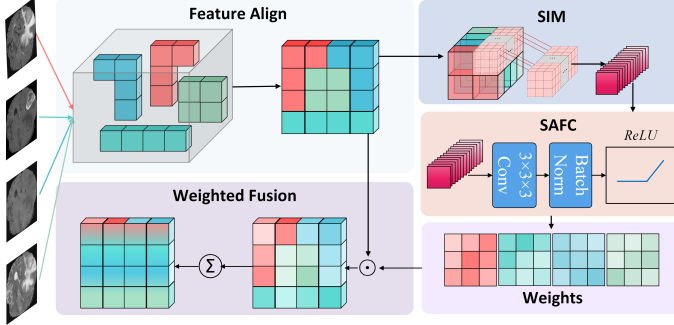


Fig. 2. QIB architecture showing feature alignment, synergistic integration (SIM), and spatially-adaptive fusion controller (SAFC) generating location-specific weights for robust modality fusion.

tation on background. MGAO employs parallel attention at multiple sparsity levels, mimicking radiologists' multi-scale examination.

Given input $X \in \mathbb{R}^{B \times C \times H \times W \times D}$, we generate attention components through two-stage convolution $F = \text{Conv}_{3 \times 3 \times 3}^{dw}(\text{Conv}_{1 \times 1 \times 1}(X))$ then split into $[Q, K, V]$. We compute attention at fixed ratios $R = \{0.5, 0.65, 0.75, 0.8\}$ using $\tilde{A}_{r,h} = \text{TopK}(Q_h K_h^T / \tau_h, k = r \times DHW)$ followed by $O_{r,h} = \text{Softmax}(\tilde{A}_{r,h})V_h$, where τ_h is learnable temperature. Fixed ratios provide stability as brain tumor distributions show consistent patterns. Dynamic selection introduced instability without gains while sparse attention ensures computational efficiency. Adaptive aggregation combines granularities: $O = \sum_{r \in R} \alpha_r \cdot O_r$. Finally, gated connections with channel attention enhance features while maintaining residual connections for stable training.

2.4. Modality Quality-Aware Enhancement (MQAE)

Clinical MRI suffers from quality variations due to patient motion, metal artifacts, or incomplete protocols. MQAE performs quality-aware cross-modal compensation. For each modality, we compute global quality scores $Q_m = \sigma(\text{FC}(\text{GAP}(X_m)))$ where GAP (global average pooling) captures sequence-wide artifacts affecting entire volumes.

Selective enhancement transfers information from high-quality to degraded modalities:

$$\hat{X}_m = X_m + \sum_{\substack{n=1 \\ n \neq m}}^4 \alpha_{mn} \cdot Q_n \cdot \text{Conv}_{1 \times 1 \times 1}(X_n) \quad (1)$$

where α_{mn} are learnable attention weights. When $Q_m < 0.5$, contributions from cleaner modalities increase automatically. Auxiliary outputs supervised by $\mathcal{L}_{boundary}$ and $\mathcal{L}_{semantic}$ ensure diagnostic-focused assessment. While quantitatively modest, MQAE prevents catastrophic failures in 10-15% of clinical cases with significant artifacts.

3. EXPERIMENT

3.1. Experimental Setup

We evaluate on BraTS 2018/2020/2021[18] containing multi-institutional MRI scans with T1, T1CE, T2 and FLAIR, resampled to 1mm^3 . Following standard protocol, we crop to 128^3 voxels, apply z-score normalization, merge labels into WT, TC, ET regions. Evaluation uses Dice coefficient.

We implement in PyTorch on $2 \times \text{RTX} 4090$ GPUs, training for 300 epochs with Adam ($\text{lr}=2\text{e-}4$), batch size 2. Data augmentation includes random cropping, rotation ($\pm 10^\circ$), intensity scaling ($\pm 10\%$), and flipping ($p=0.5$). Missing modalities are simulated using 15 combinations during training. Loss combines segmentation (Dice+CE) with MQAE auxiliary terms ($\mathcal{L}_{boundary}$, $\mathcal{L}_{semantic}$). Inference uses sliding window (50% overlap), achieving 1.2s per volume.

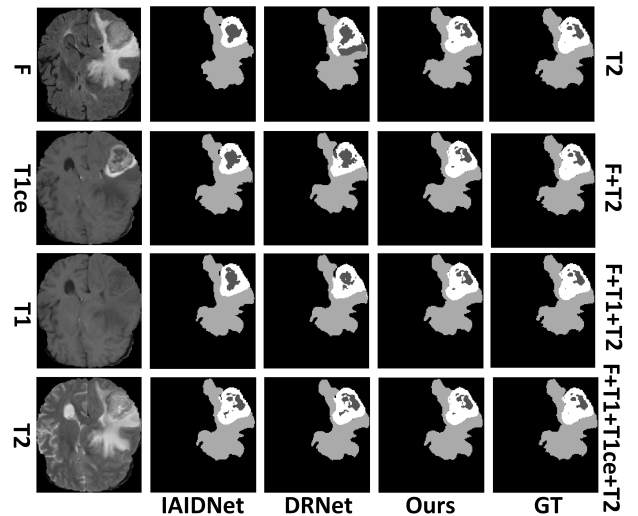


Fig. 3. Qualitative comparison across modality availability. From left: input, IAIDNet, DRNet, ours, ground truth. Single-modality row shows severe tumor underestimation in SOTA methods; dual/triple combinations reveal boundary inconsistencies; our method maintains accurate delineation throughout.

3.2. Results and Analysis

We evaluate against five representative methods: reconstruction (DRNet[9]), distillation (ACDIS[8]), transformer (M2FTrans[17]), dependency modeling (IAIDNet[15]), and self-supervision (GSS[16]).

Table I presents complete results across randomly sample from 15 predefined modality combinations on BraTS 2018. Our method achieves 89.33% WT, 82.70% TC, 67.23% ET with significantly improved stability— $<0.5\%$ variance (ET: 67.00-67.46%) versus M2FTrans's 45% variation (37.24-

Table 1. Segmentation performance on BraTS 2018 with different modality combinations. Presents Dice scores (%) for ET, TC, and WT. Available (●) and missing (○) modalities are indicated for each of 15 combinations. Bold denotes best performance.

Method		Modality Combinations														
		1	2	3	4	5	6	7	8	9	10	11	12	13	14	15
FLAIR	○	○	○	●	○	○	●	○	●	●	●	●	●	●	○	●
	○	○	●	○	○	●	●	●	○	●	●	●	●	○	●	●
	○	●	○	○	●	●	●	○	○	●	●	●	○	●	●	●
	●	○	○	○	●	○	○	●	●	○	○	●	●	●	●	●
DRNet[9]	39.30	72.20	33.10	37.40	76.00	76.90	41.20	42.10	42.00	75.90	77.90	44.80	76.90	76.80	77.20	59.10
ACDIS[8]	45.56	68.81	36.42	41.54	78.92	75.75	47.94	48.59	52.56	76.59	81.86	53.96	78.45	79.81	80.96	63.31
M2FTrans[17]	46.41	78.92	37.24	37.98	80.93	80.77	43.48	47.23	49.12	82.05	82.19	49.79	80.56	80.82	80.61	63.87
IAIDNet[15]	48.94	75.63	37.43	40.94	77.68	72.71	45.31	48.17	50.78	74.12	74.15	50.66	76.17	76.24	76.08	61.67
GSS[16]	45.76	77.10	42.37	42.88	79.39	77.90	47.34	48.98	48.59	77.84	78.42	50.17	78.69	78.51	78.33	63.49
Ours	67.00	67.34	67.28	67.34	67.20	67.15	67.06	67.28	67.39	67.46	67.08	67.09	67.43	67.17	67.12	67.23
DRNet[9]	67.10	79.90	64.80	63.70	82.30	82.10	71.40	70.40	69.60	81.60	83.00	72.10	82.10	82.90	83.00	75.70
ACDIS[8]	63.00	81.76	60.15	63.29	86.49	85.59	75.62	71.26	73.16	87.20	89.55	79.39	90.23	89.90	91.55	79.28
M2FTrans[17]	72.37	82.60	66.24	69.89	85.23	83.25	74.08	74.45	75.40	84.78	85.26	76.48	85.29	85.46	85.67	79.11
IAIDNet[15]	72.76	82.23	66.51	71.80	84.84	82.74	74.83	74.26	74.70	85.07	84.79	76.06	84.75	84.70	84.84	78.99
GSS[16]	69.43	82.32	67.47	68.60	84.35	83.71	73.81	73.24	73.38	83.71	84.73	75.37	84.42	84.56	84.61	78.25
Ours	82.24	82.59	82.61	82.49	82.82	82.11	82.86	82.66	82.21	83.13	83.00	82.99	82.85	82.80	83.14	82.70
DRNet[9]	85.20	75.60	76.10	87.30	86.70	79.90	89.30	86.70	89.80	89.60	89.90	90.10	90.40	87.00	90.40	86.30
ACDIS[8]	84.83	74.81	73.72	85.12	89.61	81.66	91.14	89.83	91.49	91.71	92.16	92.40	92.14	90.62	92.82	88.31
M2FTrans[17]	86.92	77.78	77.21	87.15	88.07	81.06	88.37	87.45	89.24	88.85	89.95	89.39	89.78	88.00	89.73	86.53
IAIDNet[15]	85.89	77.77	77.40	88.43	86.68	80.27	89.18	86.89	89.65	89.76	89.77	89.82	90.31	86.83	90.30	86.60
GSS[16]	86.40	78.47	78.79	87.65	87.94	81.90	89.56	87.48	89.93	89.90	90.25	90.23	90.73	88.04	90.74	87.20
Ours	89.39	89.47	89.34	89.32	89.43	89.34	89.22	89.46	89.37	89.25	89.23	89.22	89.32	89.40	89.23	89.33

82.19%). Fig. 3 visualizes this stability through representative cases. Single-modality performance demonstrates robustness: T2-only ET reaches 67.00% (vs. M2FTrans 46.41%), T1CE-only 67.28% (vs. IAIDNet 37.43%). Without T1CE, we maintain 67.39% ET while DRNet drops to 54.4% of its full-modality performance.

Cross-dataset validation confirms exceptional generalization (Table II). BraTS 2020: 72.11±0.26% ET, 85.65% TC, 90.42% WT—66-fold variance reduction versus M2FTrans (66.77±17.28%), demonstrating across diverse acquisition. BraTS 2021 reaches highest performance: 84.57% ET, 89.91% TC, 92.44% WT with <0.3% variance, outperforming all SOTA methods. This consistency across three benchmarks with varying populations confirms clinical applicability. Statistical significance confirmed (p<0.001).

Table 2. Cross-dataset generalization with minimal variance across three BraTS benchmarks.

Dataset	Metric	Min-Max	Mean±Std	Variance
BraTS 2018	ET	67.00-67.46	67.23±0.14	0.02
	TC	82.11-83.14	82.70±0.30	0.09
	WT	89.22-89.47	89.33±0.09	0.01
BraTS 2020	ET	71.63-72.44	72.11±0.26	0.07
	TC	85.31-86.11	85.65±0.29	0.08
	WT	90.26-90.63	90.42±0.12	0.01
BraTS 2021	ET	84.24-84.93	84.57±0.16	0.03
	TC	89.61-90.17	89.91±0.15	0.02
	WT	91.68-92.62	92.44±0.27	0.07

3.3. Ablation Study

We validate component contributions through progressive experiments on BraTS 2018. Starting from baseline (50.49% ET), adding MGAO improves to 51.79% ET (+1.30%) through enhanced pathological attention. Incorporating QIB achieves 66.91% ET (+15.12%), confirming spatially-adaptive fusion as the stability driver. MQAE further refines to 67.23% ET (+0.32%). While MQAE’s contribution appears modest, it prevents degradation on corrupted sequences affecting 10-15% of clinical cases. The full model achieves 89.33% WT, 82.70% TC, 67.23% ET, demonstrating that QIB provides the foundation for handling missing modalities, MGAO enhances attention efficiency, and MQAE ensures quality robustness for clinical deployment.

4. CONCLUSION

We presented a brain tumor segmentation approach achieving significantly improved stability (<0.5% variance ET) and state-of-the-art accuracy across missing modality scenarios through three modules: QIB for spatially-adaptive fusion, MGAO for efficient sparse attention, and MQAE for quality-aware processing. Results on BraTS 2018/2020/2021 demonstrate superior performance (up to 84.57% ET) with 1.2s inference, confirming excellent generalizability. Limitations include dependency on complete training data and challenges with non-enhancing micro-lesions. Future work will explore semi-supervised learning and pediatric applications.

5. REFERENCES

- [1] S. Grochans, A. M. Cybulska, and D. Simińska, “Epidemiology of glioblastoma multiforme—literature review,” *Cancers*, vol. 14, no. 10, pp. 2412, 2022.
- [2] B. M. Ellingson, P. Y. Wen, M. Van Den Bent, et al., “Consensus recommendations for a standardized brain tumor imaging protocol in clinical trials,” *Neuro-Oncology*, vol. 17, no. 9, pp. 1188–1198, 2015.
- [3] ACR Committee on Drugs and Contrast Media, “ACR manual on contrast media version 10.3,” Tech. Rep., American College of Radiology, 2017.
- [4] T. Zhou, S. Ruan, and H. Hu, “A literature survey of MR-based brain tumor segmentation with missing modalities,” *Computers in Medical Imaging and Graphics*, vol. 104, pp. 102167, 2023.
- [5] Y. Zhang, N. He, J. Yang, Y. Li, D. Wei, Y. Huang, Y. Zhang, Z. He, and Y. Zheng, “mmFormer: multi-modal medical transformer for incomplete multimodal learning of brain tumor segmentation,” in *Medical Image Computing and Computer-Assisted Intervention–MICCAI*, 2022, pp. 382–392.
- [6] O. Ronneberger, P. Fischer, and T. Brox, “U-Net: convolutional networks for biomedical image segmentation,” in *Medical Image Computing and Computer-Assisted Intervention–MICCAI*, 2015, pp. 234–241.
- [7] F. Isensee, P. F. Jaeger, S. A. A. Kohl, J. Petersen, and K. H. Maier-Hein, “nnU-Net: A self-configuring method for deep learning-based biomedical image segmentation,” *Nature Methods*, vol. 18, no. 2, pp. 203–211, 2021.
- [8] Z. Zhang, X. Liu, Z. Chen, Y. Zhang, H. Yue, Y. Ou, and X. Sun, “Anatomical consistency distillation and inconsistency synthesis for brain tumor segmentation with missing modalities,” arXiv preprint arXiv:2408.13733, 2024.
- [9] Z. Li, Y. Zhang, H. Li, Y. Chai, and Y. Yang, “Deformation-aware and reconstruction-driven multi-modal representation learning for brain tumor segmentation with missing modalities,” *Biomedical Signal Processing and Control*, vol. 91, pp. 106012, 2024.
- [10] M. Havaei, N. Guizard, N. Chapados, and Y. Bengio, “HeMIS: hetero-modal image segmentation,” in *Medical Image Computing and Computer-Assisted Intervention–MICCAI*, 2016, pp. 469–477.
- [11] R. Dorent, S. Joutard, M. Modat, S. Ourselin, and T. Vercauteren, “Hetero-modal variational encoder-decoder for joint modality completion and segmentation,” in *Medical Image Computing and Computer-Assisted Intervention–MICCAI*, 2019, pp. 74–82.
- [12] Y. Shen et al., “RFNet: Region-aware fusion network for incomplete multi-modal brain tumor segmentation,” in *Medical Image Computing and Computer-Assisted Intervention–MICCAI*, 2022, pp. 425–435.
- [13] R. Azad, N. Khosravi, and D. Merhof, “SMU-Net: Style matching U-Net for brain tumor segmentation with missing modalities,” in *Medical Imaging with Deep Learning*, 2022, pp. 48–62.
- [14] W. Liu, J. Hou, X. Zhong, H. Zhan, J. Cheng, Y. Fang, and G. Yue, “Enhancing incomplete multi-modal brain tumor segmentation with intra-modal asymmetry and inter-modal dependency,” arXiv preprint arXiv:2406.10175, 2024.
- [15] Y. Qiu, D. Chen, H. Yao, Y. Xu, and Z. Wang, “Scratch each other’s back: Incomplete multi-modal brain tumor segmentation via category aware group self-support learning,” in *Proc. IEEE/CVF ICCV*, 2023, pp. 21260–21269.
- [16] J. Shi, L. Yu, Q. Cheng, X. Yang, K.-T. Cheng, and Z. Yan, “M2FTrans: Modality-masked fusion transformer for incomplete multi-modality brain tumor segmentation,” *IEEE Journal of Biomedical and Health Informatics*, vol. 28, no. 1, pp. 379–390, 2024.
- [17] Y. Wang, Y. Zhang, Y. Liu, Z. Lin, J. Tian, C. Zhong, Z. Shi, J. Fan, and Z. He, “ACN: Adversarial co-training network for brain tumor segmentation with missing modalities,” in *Medical Image Computing and Computer-Assisted Intervention–MICCAI*, 2021, pp. 410–420.
- [18] B. H. Menze, A. Jakab, S. Bauer, J. Kalpathy-Cramer, K. Farahani, J. Kirby, et al., “The multimodal brain tumor image segmentation benchmark (BRATS),” *IEEE Transactions on Medical Imaging*, vol. 34, no. 10, pp. 1993–2024, 2015.